

Domain Adaptive Segmentation of Electron Microscopy with Sparse Point Annotations

Dafei Qiu
College of Computer Science and Technology
Huaqiao University, China

Jiajin Yi
Meitu, Inc.
Xiamen, China

Jialin Peng*
Xiamen Key Laboratory of CVPR
Huaqiao University, China
2004pjl@163.com

Abstract—Accurate segmentation of organelle instances is essential for electron microscopy analysis. Despite the outstanding performance of fully supervised methods, they highly rely on sufficient per-pixel annotated data and are sensitive to domain shift. Aiming to develop a highly annotation-efficient approach with competitive performance, we focus on weakly-supervised domain adaptation (WDA) with a type of extremely sparse and weak annotation demanding minimal annotation efforts, i.e., sparse point annotations on only a small subset of object instances. To reduce performance degradation arising from domain shift, we explore multi-level transferable knowledge through conducting three complementary tasks, i.e., *counting*, *detection*, and *segmentation*, constituting a *task pyramid* with different levels of domain invariance. The intuition behind this is that after investigating a related source domain, it is much easier to spot similar objects in the target domain than to delineate their fine boundaries. Specifically, we enforce counting estimation as a global constraint to the detection with sparse supervision, which further guides the segmentation. A cross-position cut-and-paste augmentation is introduced to further compensate for the annotation sparsity. Extensive validations show that our model with only 15% point annotations can achieve comparable performance as supervised models and shows robustness to annotation selection.

Index Terms—Domain adaptation, weak supervision, segmentation, electron microscopy, mitochondria segmentation

I. INTRODUCTION

Segmenting subcellular organelles, such as mitochondria instances, from large-scale electron microscopy (EM) (Fig. 1) is an indispensable task for many neuroscience research and clinical studies [1]. While state-of-the-art automatic segmentation methods are based on supervised learning [2], [3], the widespread label scarcity and data distribution shift (also known as *domain shift*) in practical scenarios usually preclude their applications. Particularly, EM images of different tissues/species show significantly different contents and appearances, which result in large domain shift. The various types of electron microscopes further increase the image diversity. While supervised training on each domain will reach highest performance, collecting sufficient data labeled by experts for model training is usually prohibitive.

To alleviate the heavy annotation burden and label scarcity on an unexplored target domain, a promising solution is to conduct domain adaptation (DA), which leverages a related but well annotated source domain and bridges the domain

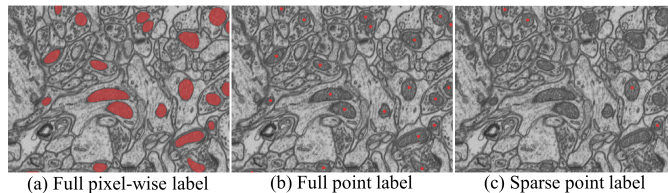


Fig. 1. Comparison of the introduced sparse point annotation with other types of annotations for mitochondria in EM images.

gap by learning domain-invariant representations [4]. Recently, unsupervised domain adaptation (UDA), assuming completely no labels on the target domain, has been extensively developed and also has made impressive progress [5]–[8] on various tasks. However, for most challenging segmentation tasks that involve high-dimensional and structured prediction, UDA approaches are far from practical usage due to the significantly low performance compared to the fully supervised counterparts. One direct way to promote the performance is to conduct semi-supervised domain adaptation (SDA) [9]. However, this strategy will significantly increase data annotation burden and delay the model deployment. Moreover, dense annotations may contain redundancy, especially for delineating subcellular organelle instances. For practical usage, it is desirable to devise a domain adaptive segmentation method that can achieve sufficiently high performance with least annotation cost.

In this study, we consider a novel class of *weakly-supervised domain adaptation (WDA)* setup, assuming that the target training data has sparse center-point annotations on a randomly-sampled small proportion (e.g., 15%) of mitochondria instances. Compared to fully pixel-wise annotation and full point annotation shown in Fig. 1, our *sparse point annotation* is extremely efficient and can be accomplished by non-expert with minimal cost in several minutes. However, this WDA setup is very challenging in comparison with fully-supervised and semi-supervised settings due to the *sparse instance coverage*, *missing information about object boundaries and appearances*, and *the only availability of labels for the positive class*. Compared to other weakly-supervised scenarios [3] that assume the availability of location cues for all instances (e.g., bounding boxes, scribbles, and full center points for all instances), this sparse point annotation setup is

The first two authors contributed equally.

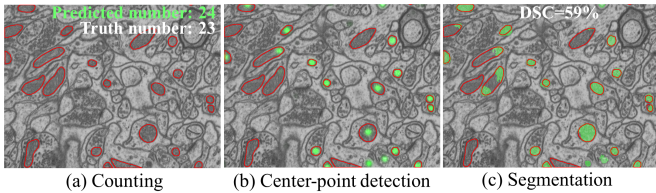


Fig. 2. Comparison of source models of different tasks when directly applying on the target domain. Red: ground truth; Green: model predictions.

also much more challenging due to missing location cues for most instances and missing background information.

To address the domain-adaptive segmentation of mitochondria instances with sparse point annotations, we introduce a novel multi-task learning framework, namely WDA-Net, which takes advantage of the correlations among *instance counting*, *center detection*, and *segmentation*, three correlated tasks with different levels of domain invariance, for multi-level domain alignment. A basic observation is that, given the extremely sparse center point annotation, global counting information can enhance center point detection, while center point locations can further greatly boost the segmentation process. Moreover, with the knowledge from a related source domain, it is much easier to roughly count and locate similar objects in an unlabeled target domain than precisely delineating object boundaries. Given these observations, we use the number estimates from a counting network trained on the source domain as a soft global prior for the cross-domain center-detection task, which is further employed to guide the cross-domain segmentation process with only sparse point supervision. Moreover, the detection and segmentation tasks are bridged by sharing semantic features and the estimated background. While the center detection task with sparse point supervision is presented as a weighted center regression problem, the counting network directly predicts the number of object instances. Moreover, we compensate the annotation sparsity with a cross-location cut-and-paste augmentation. Various validations are conducted for comparative analysis, ablation study and influence analysis of annotation selections.

II. RELATED WORK

Supervised segmentation. Compared to classical machine-learning based methods [10], [11], deep FCNs, especially U-Net and its variants, have shown strikingly higher performance [12]–[15]. Given the limited computation resources in practical applications, Peng *et al.* [12] introduced a lightweight 2D CS-Net with novel hierarchical dimension-decomposed (HDD) convolutions and obtained state-of-the-art (SOTA) performance for both mitochondria and nuclei segmentation.

Weakly-supervised segmentation. Full point annotation as weak labels has been considered [16], [17] for cell image segmentation. For nuclei segmentation in histopathology images, Qu *et al.* [18] also considered partial point annotation and used an extended Gaussian mask and self-training to learn more center points and backgrounds. Then, they explored pseudo labels estimated from Voronoi partition and clustering and

used a dense conditional random field (CRF) loss for refinement. Chen *et al.* [19] utilized sparse points on both nuclei and the background and converted the task into super-pixel classification with a few super-pixels labeled. Compared to the densely distributed nuclei, mitochondria are usually sparsely distributed with large shape variance in EM images, making the Voronoi partition/clustering/super-pixel segmentation be less efficient. Different from previous studies, we focus on cross-domain segmentation with sparse point supervision.

Domain-adaptive segmentation. The main idea behind most DA methods is to minimize the discrepancy between the feature distributions of the source and target data by various strategies, such as adversarial learning [6] and reconstruction learning [7]. The AdaptSegNet in [6] conducted domain alignment in the label space with adversarial learning and has shown SOTA performance in many tasks. For cross-domain EM image segmentation, the Y-Net in [20] learned domain invariant features that can reconstruct both the source and target images. Peng *et al.* [8] introduced DAMT-Net and has obtained SOTA performance by exploring multi-space domain alignment. Another class of strategy is to conduct self-training on pseudo labels of the domain data [21], which does not directly conduct domain alignment. While self-training based methods show promising results, they highly rely on the domain gap and the strategy to select confident pseudo labels.

For cross-domain multi-class segmentation, Paul *et al.* [22] considered image-level labels and per-class point annotation. However, category information is not informative for binary mitochondria segmentation. Xu *et al.* [23] investigated bounding-box annotations and obtained impressive results for cross-domain liver segmentation. However, it is still laborious to manually annotate the bounding-boxes of a large amount of object instances in EM images. In contrast, the sparse point annotation is much easier to collect, even by non-experts. To the best of my knowledge, we are the first study that uses sparse point annotation for domain-adaptive segmentation.

III. METHOD

To achieve accurate cross-domain segmentation with minimal annotation cost, we investigate the domain adaptation with extremely sparse center-point annotations. In the considered WDA setting, we have an almost unlabeled target domain \mathcal{D}_t with only sparse point annotation $\bar{c}^t \in \{0, 1\}^{H,W}$, taking 1 only at the center of a few mitochondria in the target image $x^t \in \mathbb{R}^{H,W}$ as shown in Fig. 1 (d). H and W are the image height and width, respectively. Moreover, we are provided with a fully labeled source domain \mathcal{D}_s with per-pixel label $y^s \in \{0, 1\}^{H,W}$ for each source image x^s . Additionally, we also define an auxiliary source label image $c^s \in \{0, 1\}^{H,W}$, which takes 1 at the mass center of each mitochondrion in x^s .

Figure 3 presents an overview of the proposed WDA-Net, which is a multi-task deep network that takes advantage of the relations among counting, center detection, and segmentation, three closely-related tasks but with different levels of domain invariance. The WDA-Net comprises a detection-segmentation

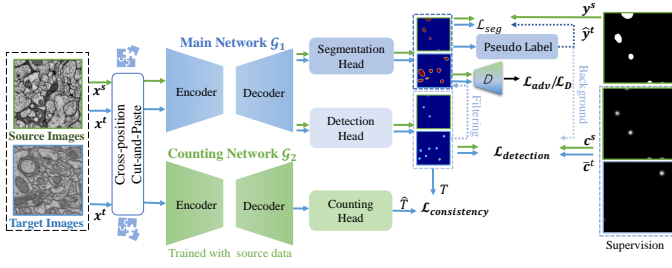


Fig. 3. Overview of the proposed WDA-Net. Three complementary tasks with different levels of domain invariance are conducted. The auxiliary counting task guides the center-point detection task, which helps locate mitochondria and filter out false positives.

network \mathcal{G}_1 and an auxiliary counting network \mathcal{G}_2 . The network \mathcal{G}_1 is a two-head convolutional network, consisting of a segmentation head that predicts the segmentation map p for each input image x , and a center detection head that predicts a heat-map \hat{d} , peaking at centers of mitochondria in the input image x . Since the counting head lacks full supervision signal under the sparse point annotation, we introduce a rough counting prior through the counting network \mathcal{G}_2 , which directly predicts the number of mitochondria and is pre-trained only on the source domain. Despite the existence of domain shift, the prediction of the counting network with sufficient data augmentation can still provide useful guidance to the heatmap regression in the detection task, especially at the early training stage. Intuitively, roughly counting the number of the object instances with source domain knowledge is much easier than pixel-wise all objects. An example is shown in Fig. 2. Therefore, we enforce a soft consistency constraint between the detection and counting predictions.

A. The Segmentation Task

The segmentation head of the WDA-Net takes advantage of both pseudo-label learning and adversarial learning to enhance the supervision from the target domain and minimize the domain discrepancy. Given a source segmentation model, we explore pixel-wise labels in the source domain and pseudo-labels in the target domain to capture more complete content of the mitochondria. The corresponding loss is written as,

$$\mathcal{L}_s = \frac{1}{|\mathcal{D}_s|} \sum_{x^s} L_{ce}(p(x^s), \mathbf{y}^s) + \frac{1}{|\mathcal{D}_t|} \sum_{x^t} L_{ce}(p(x^t), \hat{\mathbf{y}}^t) \quad (1)$$

where L_{ce} denotes the cross-entropy loss function, $p(\cdot)$ denotes the probability outputs of the segmentation head, $\mathbf{y}^s \in \{0, 1\}^{H,W,L}$ ($L=2$) is the one-hot encoding of y^s and takes an one-hot vector at each pixel x_i^s , and $\hat{\mathbf{y}}^t$ is the one-hot representation of the pseudo-labels for the target image x^t and takes $\mathbf{0}$ at regions with null pseudo-labels. While the source labels are available, pseudo-labels are generated with self-training to approximate true labels in the target domain.

Pseudo-label learning. To boost the segmentation with the unlabeled target data, we augment the segmentation pipeline with domain-adaptive pseudo-labeling in the target domain (the second term in Eq. 1), which selects predictions with high

confidence on unlabeled regions as pseudo-labels. Rather than simply thresholding the prediction $p(x^t)$ for extracting pseudo-labels [3], we select pseudo-labels by exploring entropy [3], [24], [25] and introduce an entropy-based criteria. The pseudo-label \hat{y}^t at the i th pixel for the class l is estimated as follows,

$$\hat{y}_{i,l}^t = \begin{cases} 1, & \text{if } l = \arg \max_{\bar{l}} p_{i,\bar{l}}^t \text{ and } E(p_i^t) < v_l \\ 0, & \text{otherwise} \end{cases} \quad (2)$$

where $p_{i,l}^t$ is the abbreviation of $p(x^t)_{i,l}$, $p_i^t = [p_{i,1}^t, p_{i,2}^t, \dots, p_{i,L}^t]^T$, $E(\cdot)$ denotes the entropy, and v_l is a threshold over the entropy score for the l th class,

$$v_l = D_K\{E(p_i^t) \mid x_i^t \in \mathcal{D}_t, l = \arg \max_{\bar{l}} p_{i,\bar{l}}^t\} \quad (3)$$

where D_K denotes the K th decile. In our experiment, we set $K=8$ and select the top 80% most confident label measured in the entropy as pseudo labels.

Adversarial learning. Since domain shift will lead to degraded performance when directly applying the source model on the target data, we employ adversarial learning [6] in the segmentation output-space. Concretely, a discriminator D formed as a fully convolutional network is imposed to distinguish whether the input is the prediction of a source image or a target image. For model training, we alternatively train a domain discriminator (D) by minimizing a discriminator loss \mathcal{L}_D [6], and update \mathcal{G}_1 jointly with the segmentation loss \mathcal{L}_{seg} and the additional guidance from an adversarial loss \mathcal{L}_{adv} [6], which minimizes the distribution discrepancy between the target domain and the source domain. The adversarial learning helps adapt the source model to the target data through learning domain-invariant features and also provides a relatively sound model for initializing pseudo-labeling.

B. Center Detection with Sparse Point Supervision

To take advantage of the sparse point supervision $\{\bar{c}^t\}$ on the target domain, we train an auxiliary regression-based detection head, which can predict activation maps for mitochondria locations. The detection task influences the segmentation both in implicit and explicit ways. First, the detection network influences the segmentation network by sharing most feature layers. Second, the predicted activation maps help discover informative pixels for the segmentation and the peaks of the activation maps indicate the locations of mitochondria instances. The loss function for detection is defined as follows,

$$\mathcal{L}_d = \frac{1}{|\mathcal{D}_s|} \sum_{x^s,i} (1 + \lambda \beta_i^s) (\hat{d}_i^s - d_i^s)^2 + \frac{1}{|\mathcal{D}_t|} \sum_{x^t,i} (w_i + \lambda \beta_i^t) (\hat{d}_i^t - \bar{d}_i^t)^2 \quad (4)$$

where d^s is the ground truth heatmap ($d^s = G_{\sigma_1} * c^s$) of c^s , G_{σ_1} is the Gaussian kernel with bandwidth σ_1 , and \hat{d}^s denotes the estimated heat map for x^s ; \bar{d}^t is the ground truth heatmap ($\bar{d}^t = G_{\sigma_1} * \bar{c}^t$) of the sparse center-annotations \bar{c}^t , and \hat{d}^t denotes the estimated heatmap for the target image x^t . Since we only have labels on partial center points in the target domain, we include a spatial weight map w , only taking

positive values on the estimated background (i.e., the regions with $p_{i,1}^{x^t} < \rho$, where ρ is set as 0.1 in the experiments) from the segmentation prediction and the estimated foreground (i.e., the regions with $\bar{d}_i^t > 0$). For the pixel i ,

$$w_i = \begin{cases} 1 & p_{i,1}^{x^t} < \rho \text{ or } \bar{d}_i^t > 0 \\ 0 & \text{otherwise} \end{cases} \quad (5)$$

Thus, for a target image, the loss in Eq. (4) is essentially computed on partial regions, neglecting regions with high uncertainty. Since we have high confidence about the true label in a small neighborhood of the labeled center points, we include an additional weight $\lambda\beta$ in Eq. (4) with $\beta^s = G_{\sigma_2} * c^s$ and $\beta^t = G_{\sigma_2} * \bar{c}^t$. In our experiment, σ_2 is set to be smaller than σ_1 since we have high confidence in a small neighborhood of each annotated point. The detection prediction is also used to filter out false positives with connected component analysis.

C. Counting as a Global Prior

While the detection head is designed to locate mitochondria centers in the target domain, the cross-domain training procedure lacks constraint with sparse point annotation only for the foreground class, especially at the early training stage. To address this issue, we introduce a counting task, which involves learning global-level knowledge and is expected to be more robust to domain shift, and regularize the detection with a novel counting consistency constraint. Specifically, we utilize the labeled source data to train a counting network \mathcal{G}_2 , which is an encoder-decoder network and initialized with model parameters from the segmentation network. Rather than regressing the heatmap of mitochondria locations as the detection network, the counting network directly estimates the number of mitochondria in each input image. To improve the generalization ability of the counting model, we use multi-scale input and diverse data augmentation. When applying the counting model \mathcal{G}_2 to a target image x^t , we can obtain an estimated number of mitochondria instances in x^t and denote it as $T(x^t)$, which can act as a rough global prior. Given the predicted activation map \hat{d}^t of the detection branch of the main network \mathcal{G}_1 for x^t , we can also obtain an estimated number of mitochondria instances in x^t and denote it as $\hat{T}(x^t)$. In the ideal case, $\hat{T}(x^t)$ will equal to $T(x^t)$. However, there may be discrepancy between $T(x^t)$ and the ground truth due to inaccurate estimation by \mathcal{G}_2 . Thus, we introduce a consistency loss with a small soft margin ε (3 in our experiment) to enforce soft consistency between counting and detection predictions.

$$\mathcal{L}_c = \frac{1}{|\mathcal{D}_t|} \sum_{x^t} \max\left(0, (T - \varepsilon) - \hat{T}\right) + \max\left(0, \hat{T} - (T + \varepsilon)\right) \quad (6)$$

D. Cross-Position Cut-and-Paste Label Augmentation

A significant challenge of exploring supervision in the target domain is the extremely sparsity of the point annotations. To compensate for this, we introduce a cross-position cut-and-paste augmentation (CP-Aug) strategy similar to cutmix [26]. However, the cropped patches are not necessarily pasted in the same position with the aim to increase the density of point

annotations. Given two images (x_A^t, \bar{c}_A^t) and (x_B^t, \bar{c}_B^t) from the target domain, we aim to generate a new image (x_C^t, \bar{c}_C^t) by cutting a rectangular region (256×256 in our experiments) with largest number of annotation points in x_A^t and pasting it to a rectangular region of the same size but with few number of annotation points in x_B^t . The synthesized images have more annotated points and will be used in model training.

E. Overall Optimization and End-to-End Learning

For model training, we alternatively train the domain discriminator (D) by minimizing the discriminator loss \mathcal{L}_D [6], and update \mathcal{G}_1 . Specifically, given the discriminator D and pretrained counting network \mathcal{G}_2 , we train the main network \mathcal{G}_1 by minimizing the following loss,

$$\mathcal{L}_{obj} = \mathcal{L}_s + \lambda_a \mathcal{L}_{adv} + \lambda_d \mathcal{L}_{detection} + \lambda_c \mathcal{L}_c \quad (7)$$

where λ_a, λ_d are trade-off parameters; $\lambda_c = 1 - z/z_{max}$ decays along with iteration z , and z_{max} is the maximum iteration.

IV. EXPERIMENTS

A. Dataset and Evaluation Settings

Drosophila Data [27] were taken from *Drosophila melanogaster* third instar larva VNC using serial section Transmission Electron Microscope (ssTEM) in an anisotropic resolution of 4.6×4.6 nm/pixel with the section thickness of 45-50 nm. This image stack is of size 20×1,024×1,024.

EPFL Data [10] were taken from the hippocampus of a mouse using focused ion beam scanning electron microscope (FIB-SEM) in a resolution of 5×5×5 nm. Both the training and testing subsets are of size of 165×768×1,024.

Kasthuri++ Data [13] were taken from mouse cortex with serial section EM in a resolution of 3 × 3 × 30 nm. This dataset comprises a training subset of size 85×1,463×1,613 and a testing subset of size 75×1,334×1,553.

We evaluate our method under two source-target scenarios: 1) the adaptation from the small *Drosophila* dataset to the large EPFL dataset, and 2) the adaptation from EPFL data to Kasthuri++ data, which contains a large proportion of background and larger number of mitochondria.

Source annotation refinement (SAR). While Kasthuri++ data are labeled with accuracy, the EPFL data contain more inconsistency on the boundaries. Thus, we introduce a source annotation refinement, which employs the Geodesic Active Contour (GAC) model [28] to automatically refine the labels in the source domain while keeping the target ground truth label untouched. The GAC model can make the source annotations more consistent with image boundaries.

Evaluation metrics. We utilize both class-level measure, i.e., Dice similarity coefficient (DSC) in %, and instance-level measures, i.e., Aggregated Jaccard-index (AJI) [29] in % and Panoptic Quality (PQ) [30] in %.

Network architectures. For the backbone of the \mathcal{G}_1 network, we use a lightweight variant of U-Net, which uses the HDD unit in [12] as the basic building blocks. Besides the prediction layer, the segmentation head and detection head use one HDD layer and two HDD layers, respectively. To obtain

TABLE I
ABLATION STUDY OF THE PROPOSED WDA-NET.

Model	Detect.	Count	P-L	CP-Aug	SAR	Filter	EPFL →Kasthuri++	
							DSC(%)	PQ(%)
I							76.0	49.6
II	✓						86.3	57.1
III	✓	✓					87.5	64.5
IV			✓				81.9	55.2
V	✓		✓				89.0	67.1
VI	✓	✓	✓				89.0	68.5
VII	✓	✓	✓	✓			90.3	70.2
VIII	✓	✓	✓	✓	✓		92.1	73.6
IX	✓	✓	✓	✓	✓	✓	92.1	76.6

counting prediction from the detection output, we utilize one HDD layer followed by an integration layer for prediction. The counting network \mathcal{G}_2 has the same backbone as \mathcal{G}_1 with a integration layer for final prediction. We use the same discriminator as [8], which is a fully-convolutional network of 5 layers with channel numbers of {64, 128, 256, 512, 1}.

Parameters and training settings. We set $\lambda_a=10^{-3}$, $\lambda_d=10^{-1}$, $\lambda=3$, and $\beta=0.2$. The bandwidths σ_1 and σ_2 are set as 10 and 2, respectively. We implement the models on one 1080Ti GPU. The \mathcal{G}_1 network is trained using SGD with initial learning rate 5×10^{-5} and polynomial decay of power 0.9. The z_{max} is set to 10k and the batch size is 1. We randomly crop patches of size 512×512 as training input. Data augmentations including flipping/rotation, blur, color jitter, and the proposed CP-Aug are used. The discriminator is trained with Adam optimizer as [8]. The \mathcal{G}_2 network is initialized with parameters of the \mathcal{G}_1 network and optimized with mean squared loss and Adam optimizer. Multi-scale inputs of size 512×512 , 768×768 , and 1024×1024 obtained through crop and resampling and data augmentation including flipping/rotation, blur, and color jitter are used for training the \mathcal{G}_2 network.

B. Ablation study

Table I demonstrates the individual contributions of our key components, a) Detect.: using the detection head; b) Count: using the counting consistency constraint to the detection head; c) P-L: pseudo-label learning; d) CP-Aug: the cross-position cut-and-paste augmentation, e) SAR: the source annotation refinement with GAC; and f) Filter: connected component analysis of the segmentation with points from the detection head and also removing noise blobs with open-and-close operation. The ablation studies are conducted using 15% point annotation, namely WDA-Net (15%), for EPFL →Kasthuri++.

While the baseline Model I only conducts UDA with adversarial training [6], sequentially adding the key components results in gradually improved performance. By integrating the center detection to the Model I, we achieve a significant improvement of 10.3% in DSC, 7.5% in PQ. By introducing the counting prior constraint, we obtain further improvement, especially a large performance gain (7.4% in PQ) in detection. By comparing Model V, Model IV, and Model I, we observe that integrating the detection with the pseudo-label learning can significantly improve both the segmentation and detection

TABLE II
COMPARISON RESULTS ON DROSOPHILA DATA →EPFL DATA AND EPFL DATA →KASTHURI++ DATA.

Method	Backbone	Drosophila →EPFL			EPFL →Kasthuri++		
		DSC	AJI	PQ	DSC	AJI	PQ
NoAdapt	U-Net	57.3	39.6	26.0	70.0	52.8	42.2
Y-Net [20]		68.2	–	–	73.7	56.8	44.3
AdaptSegNet [6]	U-Net	69.9	–	–	77.4	61.5	52.9
DAMT-Net [8]		74.7	–	–	82.0	68.3	56.5
Y-Net [20]		69.6	52.2	42.6	76.7	60.0	48.9
AdaptSegNet [6]	U-Net	71.2	54.9	47.3	78.3	62.0	50.7
DAMT-Net [8]	(HDD)	75.3	59.7	47.7	83.7	70.2	57.5
WDA-Net (5%)		88.5	79.3	74.5	91.1	82.0	74.7
WDA-Net (15%)	U-Net	90.7	82.1	76.5	92.1	83.4	76.6
WDA-Net (50%)	(HDD)	91.0	83.4	77.8	92.6	84.6	77.1
WDA-Net (100%)		91.6	83.9	78.3	92.8	85.2	77.8
Supervised (Upper bound)	U-Net (HDD)	93.6	87.9	80.2	94.6	88.3	82.2

tasks, while the performance gain in PQ by only using pseudo-label learning is limited. By comparing Model VII and Model VI, we find that the CP-Aug can lead to an improvement of 1.9% in PQ. By comparing Model VIII and Model VII, we observe that the CP-Aug can obviously improve the model performance, because the EPFL data have obvious inconsistency in boundaries. Finally, the detected center points can help significantly reduce false positives, and Model IX outperforms Model VIII by 3.0% in PQ. In summary, all the proposed components can consistently improve the performance, and Detect., Count, CP-Aug, and Filter have stronger ability to improve the detection performance.

C. Comparative Experiment

Table II compares WDA-Net with SOTA UDA methods, i.e., Y-Net [20], AdaptSegNet [6], and DAMT-Net [8], and the upper bound, i.e., the supervised model on the target domain. In Table II, we also compares the proposed WDA-Net using different ratios of point annotations. Moreover, both the vanilla U-Net [2] and U-Net (HDD), i.e., the proposed lightweight variant of U-Net, are tested as the backbone network.

First, we can observe that the U-Net with HDD [12] shows better performance than the vanilla U-Net, while the model size (6.7M) of the U-Net (HDD) is only about 1/5 of the model size (34.5M) of the vanilla U-Net. Thus, in the following experiment, we use the U-Net (HDD) as the backbone. Second, for both adaptation tasks, the well-trained source models show significant performance drop when directly applying on the target domain, which indicates the severe domain shift and the sensitivity of deep network models.

Third, with extremely low annotation cost, our WDA-Net significantly outperforms the UDA counterparts and shows comparable performance with the supervised trained counterpart. By comparing the performance of our model with annotation ratios, we find that annotating on 15% instances of the target training data can already produce sound performance on the testing data. For the Drosophila III VNC→Mouse Hippocampus, the proposed WDA-Net (15%) outperforms the DAMT-Net by a large margin with only minimal annotation cost and obtains a performance of 92.8% in DSC

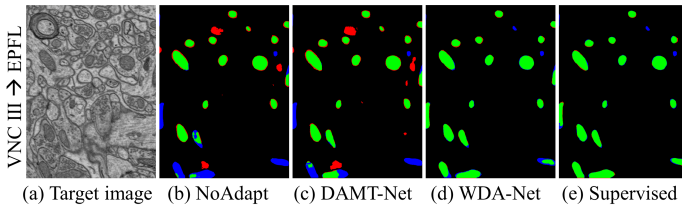


Fig. 4. Visual comparison of the proposed WDA-Net (15%) with other methods. Red: false positives; Blue: false negatives; Green: true positives.

and 78.3% in PQ, which are only 2.0% and 1.9% lower, respectively, than that of the supervised model. Similarly, for the EPFL→Kasthuri++, the proposed WDA-Net (15%) achieves the performance of 92.8% in DSC, only 1.8% lower than the supervised model, showing the benefit of our model.

Figure 4 visually compares our WDA-Net with other methods. Compared to NoAdapt, the DAMT-Net can recognize more mitochondria instances similar to the source mitochondria, but this method still has many false positives and false negatives. In contrast, with minimal annotation effort, the proposed method can significantly reduce false positives and false negatives, and shows comparable results with the fully-supervised method. Moreover, with 15% center points for the training data, our method can already produce sound results.

V. CONCLUSION

In this study, we addressed domain-adaptive mitochondria segmentation under sparse center point supervisions. Experiments on challenging benchmarks have showed that our model can produce sound performance close to the supervised counterpart with only 15% partial point supervision. The validations also showed the robustness of our model. In future work, we will consider source-free setting and explore only well-trained source models and the target data for adaptation.

REFERENCES

- [1] J. Nunnari and A. Suomalainen, "Mitochondria: in sickness and in health," *Cell*, vol. 148, no. 6, pp. 1145–1159, 2012.
- [2] O. Ronneberger, P. Fischer, and T. Brox, "U-net: Convolutional networks for biomedical image segmentation," in *International Conference on Medical Image Computing and Computer-Assisted Intervention*, 2015, pp. 234–241.
- [3] J. Peng and Y. Wang, "Medical image segmentation with limited supervision: a review of deep network models," *IEEE Access*, vol. 9, pp. 36 827–36 851, 2021.
- [4] M. Long, Y. Cao, and J. Wang, "Learning transferable features with deep adaptation networks," in *International Conference on Machine Learning*, 2015, pp. 97–105.
- [5] Y. Ganin, E. Ustinova, H. Ajakan, P. Germain, and H. Larochelle, "Domain-adversarial training of neural networks," *Journal of Machine Learning Research*, vol. 17, no. 1, pp. 2096–2030, 2016.
- [6] Y. Tsai, W. Hung, S. Schuster, K. Sohn, M. Yang, and M. Chandraker, "Learning to adapt structured output space for semantic segmentation," in *IEEE Conference on Computer Vision and Pattern Recognition*, 2018, pp. 7472–7481.
- [7] M. Ghifary, W. B. Kleijn, M. Zhang, D. Balduzzi, and W. Li, "Deep reconstruction-classification networks for unsupervised domain adaptation," in *European Conference on Computer Vision*, 2016, pp. 597–613.
- [8] J. Peng, J. Yi, and Z. Yuan, "Unsupervised mitochondria segmentation in em images via domain adaptive multi-task learning," *IEEE Journal of Selected Topics in Signal Processing*, vol. 14, no. 6, pp. 1199–1209, 2020.

- [9] S. Chen, X. Jia, J. He, Y. Shi, and J. Liu, "Semi-supervised domain adaptation based on dual-level domain mixing for semantic segmentation," in *IEEE/CVF Conference on Computer Vision and Pattern Recognition*, 2021, pp. 11 013–11 022.
- [10] A. Lucchi, Y. Li, and P. Fua, "Learning for structured prediction using approximate subgradient descent with working sets," in *Proceedings of IEEE Conference on Computer Vision and Pattern Recognition*, 2013, pp. 1987–1994.
- [11] J. Peng and Z. Yuan, "Mitochondria segmentation from em images via hierarchical structured contextual forest," *IEEE Journal of Biomedical and Health Informatics*, vol. 24, no. 8, pp. 2251–2259, 2020.
- [12] J. Peng and Z. Luo, "Cs-net: Instance-aware cellular segmentation with hierarchical dimension-decomposed convolutions and slice-attentive learning," *Knowledge-Based Systems*, vol. 232, p. 107485, 2021.
- [13] V. Casser, K. Kang, H. Pfister, and D. Haehn, "Fast mitochondria detection for connectomics," in *Medical Imaging with Deep Learning*. PMLR, 2020, pp. 111–120.
- [14] C. Xiao, X. Chen, W. Li, L. Li, L. Wang, Q. Xie, and H. Han, "Automatic mitochondria segmentation in em data using a 3d supervised convolutional network," *Frontiers in Neuroanatomy*, vol. 12, p. 92, 2018.
- [15] Z. Yuan, X. Ma, J. Yi, Z. Luo, and J. Peng, "Hive-net: Centerline-aware hierarchical view-ensemble convolutional network for mitochondria segmentation in em images," *Computer Methods and Programs in Biomedicine*, vol. 200, p. 105925, 2021.
- [16] K. Nishimura, C. Wang, K. Watanabe, D. Fei Elmer Ker, and R. Bise, "Weakly supervised cell instance segmentation under various conditions," *Medical Image Analysis*, vol. 73, p. 102182, 2021.
- [17] T. Zhao and Z. Yin, "Weakly supervised cell segmentation by point annotation," *IEEE Transactions on Medical Imaging*, vol. 40, no. 10, pp. 2736 – 2747, 2020.
- [18] H. Qu, P. Wu, Q. Huang, J. Yi, Z. Yan, K. Li, G. M. Riedlinger, S. De, S. Zhang, and D. N. Metaxas, "Weakly supervised deep nuclei segmentation using partial points annotation in histopathology images," *IEEE Transactions on Medical Imaging*, vol. 39, no. 11, pp. 3655–3666, 2020.
- [19] Z. Chen, Z. Chen, J. Liu, Q. Zheng, Y. Zhu, Y. Zuo, Z. Wang, X. Guan, Y. Wang, and Y. Li, "Weakly supervised histopathology image segmentation with sparse point annotations," *IEEE Journal of Biomedical and Health Informatics*, vol. 25, no. 5, pp. 1673–1685, 2021.
- [20] J. Roels, J. Hennies, Y. Saeyns, W. Philips, and A. Kreshuk, "Domain adaptive segmentation in volume electron microscopy imaging," in *International Symposium on Biomedical Imaging*, 2019, pp. 1519–1522.
- [21] Y. Zou, Z. Yu, B. Kumar, and J. Wang, "Domain adaptation for semantic segmentation via class-balanced self-training," in *European Conference on Computer Vision*, 2018, pp. 289–305.
- [22] S. Paul, Y.-H. Tsai, S. Schuster, A. K. Roy-Chowdhury, and M. Chandraker, "Domain adaptive semantic segmentation using weak labels," in *European Conference on Computer Vision*, 2020, pp. 571–587.
- [23] Y. Xu, M. Gong, and K. Batmanghelich, "Box-adapt: Domain-adaptive medical image segmentation using bounding boxsupervision," *IJCAI Workshop on Weakly Supervised Representation Learning*, 2021.
- [24] D.-H. Lee *et al.*, "Pseudo-label: The simple and efficient semi-supervised learning method for deep neural networks," in *Workshop on challenges in representation learning at International Conference on Machine Learning*, vol. 3, no. 2, 2013, p. 896.
- [25] A. Saporta, T.-H. Vu, M. Cord, and P. Pérez, "Esl: Entropy-guided self-supervised learning for domain adaptation in semantic segmentation," *arXiv preprint arXiv:2006.08658*, 2020.
- [26] S. Yun, D. Han, S. Chun, S. J. Oh, Y. Yoo, and J. Choe, "Cutmix: Regularization strategy to train strong classifiers with localizable features," in *IEEE/CVF International Conference on Computer Vision (ICCV)*, 2019, pp. 6022–6031.
- [27] S. Gerhard, J. Funke, J. Martel, A. Cardona, and R. Fetter, "Segmented anisotropic stsem dataset of neural tissue," 2013. [Online]. Available: <https://github.com/unidesigner/groundtruth-drosophila-vnc>
- [28] V. Caselles, R. Kimmel, and G. Sapiro, "Geodesic active contours," in *International Conference on Computer Vision*, 1995, pp. 694–699.
- [29] N. Kumar, R. Verma, S. Sharma, S. Bhargava, A. Vahadane, and A. Sethi, "A dataset and a technique for generalized nuclear segmentation for computational pathology," *IEEE Transactions on Medical Imaging*, vol. 36, no. 7, pp. 1550–1560, 2017.
- [30] A. Kirillov, K. He, R. Girshick, C. Rother, and P. Dollár, "Panoptic segmentation," in *Proceedings of the IEEE Conference on Computer Vision and Pattern Recognition*, 2019, pp. 9404–9413.